



Consideration of image processing system for high visibility of display using aerial imaging optics

Hayato Kikuta^{1,2} · Masaki Yasugi^{1,3} · Hirotsugu Yamamoto¹

Received: 30 June 2023 / Accepted: 17 November 2023 / Published online: 21 December 2023
© The Optical Society of Japan 2023

Abstract

We are researching a new display device that allows the public to experience augmented reality without wearable devices. In this paper, we implement an image processing system that improves the dynamically changing image quality deterioration, which is a problem unique to optical systems that project images on the real space, and specify the necessary system requirements from the results of verification of the effect. We quantify the characteristics of blur for each of the three primary colors defined as digital image data, and implement image processing that applies filter correction to the input image data during aerial imaging. Since the effect on image quality depends on what kind of imaging optical path is formed, we designed the device structure assuming that it will be applied to signage products, and built an experimental environment that can analyze the aerial image that the user actually sees. The image subjected to the correction process follows an optical path that forms an image in the air, and the user visually recognizes the image with emphasized edges. We compared the results of the actual aerial image and the simulation results, and clarified the system requirements for realizing an image processing system with higher correction accuracy.

Keywords Retro-reflection · Aerial display · Deconvolution processing · Point spread function

1 Introduction

In recent years, the development of virtual reality (VR) and augmented reality (AR) technologies necessitates more visually immersive user interfaces. Aerial imaging technology has the potential to be applied to these situations as a display device that expands visually in real space without a wearable device [1–3]. The technology applies optics that re-converge light from a diffuse light source onto a different space, allowing users to see visual information in a space where it isn't physically existed. There are several ways to achieve this technology, and it can be applied to devices with various added values, depending on the display size and the imaging

distance from hardware to aerial image, as shown in Fig. 1. For example, if the floating distance is large, the technology can be incorporated into large facilities and staging equipment to act as a signage display that can be experienced by an unspecified number of users [4]. Because the user sees the image in an unexpected location, such as on a moving line of motion, the display device can recognize the information more strongly and provide alerts without the risk of collision. And if the floating distance is small, for example, the technology could be embedded in a wall or table and used as an information display terminal for a specific user. The system is further applied to the user's hand as an interaction interface with aerial images by combining it with spatial position sensing technology such as an infrared camera sensor. If the image size is small, it is utilized as a button interface, and if the display size is about 10–20 in., it is utilized as a touch panel interface like a tablet device. In both cases, it is expected to be applied to factories and medical facilities as a sanitary touch interface [5–9].

The problem for applying this technology to display products is that the display resolution varies with the optical system. Depending on the accuracy of the optical element

✉ Hirotsugu Yamamoto
hirotsugu@yamamolab.science

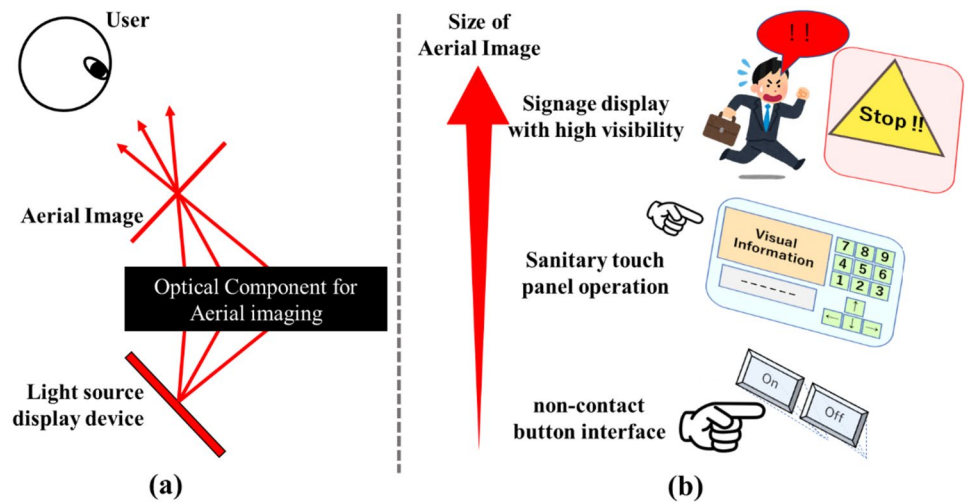
Hayato Kikuta
Kikuta.Hayato@dp.MitsubishiElectric.co.jp

¹ Utsunomiya University, Utsunomiya, Tochigi, Japan

² Mitsubishi Electric Corp., Chiyoda-ku, Tokyo, Japan

³ Fukui Prefectural University, Obama, Fukui, Japan

Fig. 1 Product application examples according to the size of the aerial image. **a** Construction concept of aerial display by optical element for aerial imaging. **b** Example of product application according to the size of the aerial image



used, the diffuse light source cannot ideally be re-converged. Unconverging light blurs aerial images and reduces sharpness. Previous studies have evaluated the sharpness of the aerial image using the distance between the aerial image and the hardware that changes as the imaging optics become larger for large aerial image as a comparison parameter, and it has been shown that the greater the distance, the greater the blurriness [10].

As previous research for the purpose of improving the display image quality of aerial images, a correction method based on the analysis of image quality changes during aerial imaging and filter control has been proposed [11]. Furthermore, in the case of an imaging method using retroreflection, it has been studied that the decrease in anisotropic sharpness, which varies depending on the configuration characteristics and color wavelength of the retro-reflection elements, can be quantified and corrected [12–14]. The characteristics of blur caused by retro-reflective elements that change according to the wavelengths of the three primary colors are quantified and converted into correction parameters for improvement. In previous studies, it has been shown that the optimal parameter selection is important by correcting the captured aerial image with each parameter and quantifying it using similarity evaluation. However, in the experimental environment of the previous research, the correction processing was only applied to the camera image taken by shooting the uncorrected aerial video, and the correction processing for the actual aerial video was not verified. The correction in the previous study is the simulation results in which blur correction processing is performed in digital image space, and it is necessary to verify the performance difference with the correction processing for the light source to the actual aerial imaging optics. Therefore, at the 12th Laser Display and Lighting Conference 2023, we implemented an image processing system that can perform blur correction on actual aerial images and presented preliminary experiments on

verification of the correction effect [15]. As a result, it was confirmed that the correction effect was qualitatively effective even for actual aerial images, and it was shown that quantitative evaluation by contrast was possible.

This paper aims to verify the blur correction effect on actual full-color aerial images and clarify the system requirements for application to aerial display products. In this experiment, we construct an imaging environment in which input light from a digital display can be imaged as an aerial image, and the aerial image can be captured by a camera. In the analysis phase, the point spread function (PSF) for each monochromatic color of light imaging display is calculated. From the obtained PSF results, a filter function that provides optimal blur correction for each color image is generated, and an image processing system is implemented to perform convolution processing on the light source image used for actual aerial imaging. In order to verify the effect of the obtained correction, the projected aerial images are compared with the simulation results obtained by performing correction processing on the captured data, and the system requirements necessary to correct the actual aerial images are considered.

2 Principles

2.1 Resolution degradation due to aerial imaging optics

There are some aerial imaging optics, we use an optical system applying retroreflection, which has high applicability to a variety of aerial display products from large to small [16–18]. Although the characteristics are different even in the case of aerial imaging optics using multiple micro-mirrors or lens arrays, the application of this technique is possible [19, 20]. Figure 2 shows the optical principles of

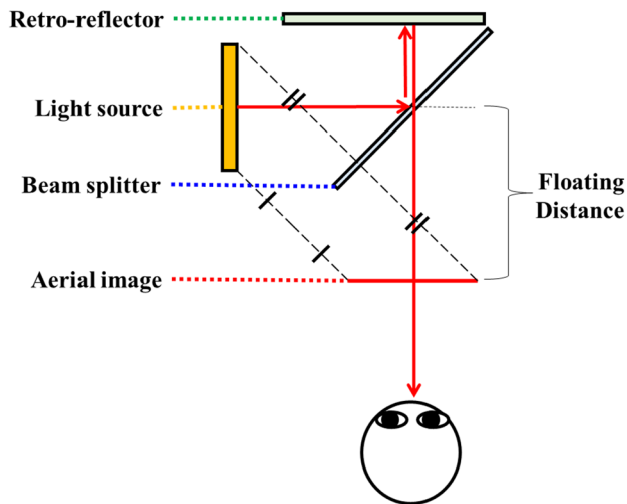


Fig. 2 Principle of aerial imaging by retro-reflection (AIRR)

the aerial imaging by retro-reflection (AIRR). The technology consists of a light source display, a beam splitter and a retro-reflector. A light source display is a diffuse display with visible light similar to a normal monitor display, etc., and the AIRR images of the same content displayed on the light source as an aerial image in a plane-symmetrical position with the beam splitter. The optical path to image in the mid-air includes transmission and reflection by the beam splitter surface, and retro-reflection by the retro-reflective material surface. Among them, the main cause of the image quality degradation is the diffraction phenomenon in retro-reflection by the retroreflective element.

As shown in Fig. 3, there are generally two ways to realize a retro-reflecting device, but both of them have an opening that can be made incident on the inside of the elements, which causes a diffraction phenomenon. The diffraction shifts the ideal retro-reflective direction of the output light, the retro-reflected light spreads. Diffraction generated from one element is known to have a relationship among its wavelength λ , aperture width d , and light divergence angle θ , as shown in Eq. (1).

$$\sin\theta = \frac{\lambda}{d} \approx \frac{x}{L} \quad (1)$$

Furthermore, when the distance L from the aperture position to the imaging position is very large compared to the aperture width d , the position deviation x due to diffraction and $\sin\theta$ are approximated using L . That blurring caused by aerial imaging is inversely proportional to the aperture width d and wavelength λ and proportional to the imaging distance L [21].

One way to achieve retro-reflection is through multiple refractions on the micro-bead shape and specular reflection on the underlying reflective layer. This method has a

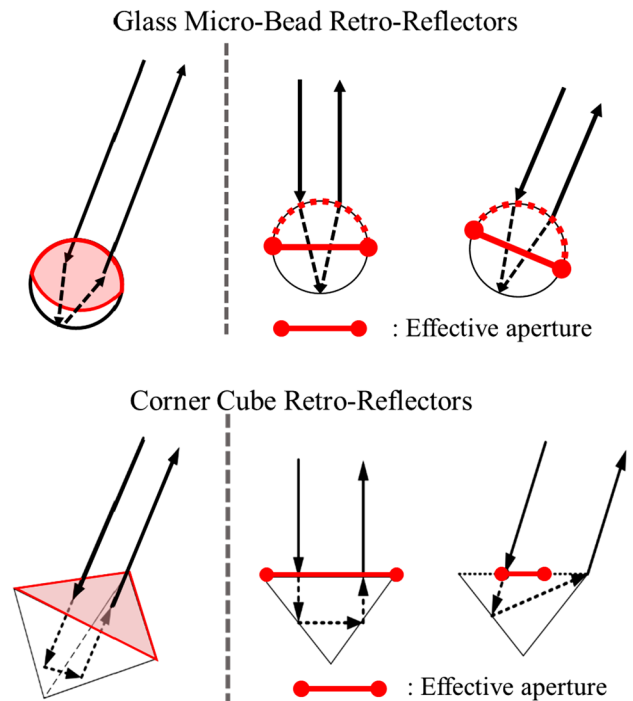


Fig. 3 Schematic diagram of changes in effective aperture width depending on the shape of the retroreflective element and the angle of incidence

constant aperture width at any angle of incidence. However, commonly distributed retro-reflectors have a small size of the element itself and a small aperture width, resulting in a significant reduction in image quality.

On the other hand, the shape often used as an aerial display product is a microprism type. It achieves retro-reflection by multiple reflections with three orthogonal reflective layers. The device size of this method is larger than that of microbeads, making it easier to maintain resolution during aerial imaging. However, since the width of diffraction varies depending on the incident angle of light, the effect of diffraction varies depending on the configuration environment of the aerial imaging optics. When the diffraction inside the retro-reflecting element becomes large, the light spreads out in proportion to the optical path from the time of retro-reflection to the time of imaging in the air, and the aerial image becomes blurred. In other words, in the structure shown in Fig. 2, if the distance between the retro-reflector and the beam splitter is designed to be minimum, the size of the blur varies depending on the floating distance from the optical system to the aerial image.

2.2 Blur analysis and correction processing

Next, we describe a method to analyze the blurring characteristic of aerial imaging optics and utilize it as a correction

parameter [12]. Due to the aforementioned reduction in resolution according to the aperture width of the retro-reflecting element, the optical system does not converge an arbitrary diffuse light source to an ideal position in space, but spreads out. That is, when a light source is applied as a flat panel display and a display device, the spread of the light can be mapped on a plane formed as an aerial image and expressed as a two-dimensional spread function. Point spread function (PSF) is commonly used to quantitatively represent factors, such as camera lens blur and camera shake, and it represents the amount of blur and its direction as a two-dimensional brightness distribution. In order to use PSF to analyze the blurring of aerial image, it is necessary to construct an environment that can be captured as a digital image with respect to the display environment in which the actual aerial image is formed. Figure 4 shows how PSF is calculated. We project a circle of radius R on a light source display and image it in the mid-air to acquire an image for use in analysis. When capturing the aerial image, we set the focal position and the depth of field in advance to match the plane to be imaged in the mid-air, and then capture the image with RAW data. We cancel the gamma correction of the image data, adjust it to be linear to the brightness, and create PSF, denoted by $h(\theta, r)$, as shown in Eq. 2.

$$h(\theta, r) = A_\lambda(\theta, R + r) - S(\theta, R + r) \tag{2}$$

In Eq. (2), the image data are represented in a polar coordinate system to map the rise in brightness that occurs outside the boundary of the more ideal edge during aerial imaging as a blur characteristic in PSF. In the case of less blurring, a steep profile can be obtained in the brightness value outside the boundary of the captured aerial image $A_\lambda(\theta, R + r)$. Conversely, when the blur is large, the brightness values have a gentle profile. In addition, this paper uses the same optical structure as our previous research, and by setting the spread of light due to diffraction to be larger than the area of the light source image, it is possible to calculate with an equation that excludes the blur from the inside of

the light source area [14]. The PSF shown on the right side of Fig. 4 is the result of calculation using Eq. (2) for an input image that has been subjected to Gaussian blur around a white circle in order to visually illustrate the measurement results. We have been able to numerically obtain the characteristics of the direction and intensity of blur on a two-dimensional surface. As mentioned above, the PSF calculation formula in this paper allows some error depending on the amount of blur in the experimental environment of aerial imaging, so the input image example in Fig. 4 does not provide a strict PSF result.

Also, as mentioned in the previous section, the magnitude of the effect of the blurring due to the diffraction phenomenon of the retro-reflecting element depends on the color wavelength of the light source. Since a typical display device emits light based on the three primary colors of red, green, and blue, the captured images of each of those three colors need to be captured and analyzed for PSF.

Then, a method to correct image quality degradation from the obtained PSF is described. PSF can be regarded as a filter function of blurring in digital image processing because it represents the properties of blurring on the aerial image plane. Therefore, by convolving an inverse function such as Eq. (3), which negates the characteristics of PSF, into the input image beforehand, it becomes possible to correct the blurring during aerial imaging.

$$g(x, y) = f(x, y) \times m(x, y) \tag{3}$$

Then, $g(x, y)$ denotes the corrected image data and $f(x, y)$ denotes the input image data, and by folding the correction function $m(x, y)$ into the input image, the corrected image can be output to the image displayed on the light source display before aerial imaging. The function $m(x, y)$ can be obtained by calculating the inverse filter from the PSF results in the frequency domain and, for digital image processing, by calculating the Wiener filter. The Wiener filter calculates the Fourier transformed M of the desired correction function in the Eq. (4).

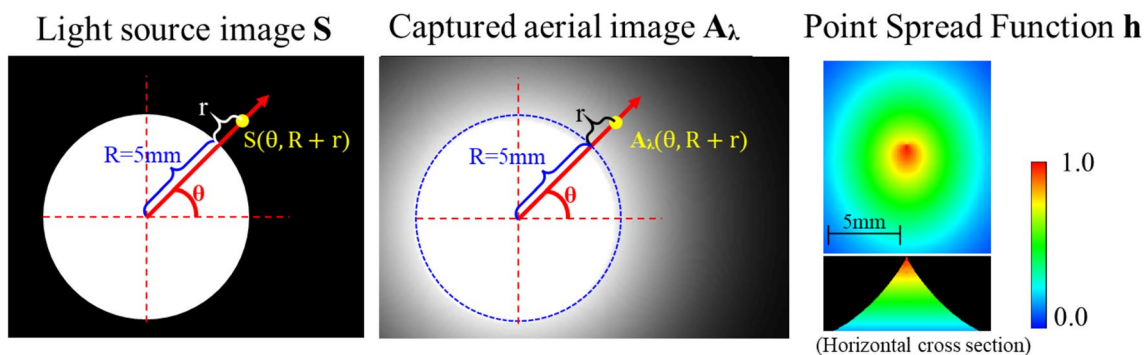


Fig. 4 PSF calculation of input image and captured aerial image

$$M = \frac{H^*}{|H|^2 + N} \quad (4)$$

where H is the result of Fourier transformation of the PSF result and N is the noise constant. For N , the higher the value, the smoother the corrected image, and the smaller the value, the finer the noise pattern appears. In this experiment, a correction function is generated by qualitatively selecting high-visibility values in the range of 0.1–0.5.

Also, as with PSF calculations, it is necessary to perform correction processing independently for each of the three primary colors emitted by full-color aerial display devices. Three input channels of image data are separated and deconvolved for each color, and the resulting corrected image is synthesized into a full-color image.

3 Experiments

3.1 Experimental setup

In this paper, it is necessary to be able to analyze the resolution of aerial images using PSF and experimentally confirm the effect of correction processing with an aerial display device with the same resolution as its characteristics. Therefore, as shown in Fig. 5, we constructed an aerial image using a high-brightness liquid crystal display (LCD) as a light source and an imaging experiment environment to capture it so that PSF analysis and corrected aerial image verification can be performed in the same environment. The input light source utilizes a high-brightness full-color LCD display (Feel World product: FW279) so that the circle display for PSF measurement of each color wavelength and the actual aerial image content can be displayed. The specifications of this LCD are that the maximum brightness is 2200 cd/m², and the peak wavelengths of each color are Red: 450nm, Green: 548nm, and Blue: 640nm. In addition, since the light source is linearly polarized, using a material that changes the ratio of reflection and transmission according to the polarization state for the beam splitter and adding a material that shifts the phase to the surface of the retro-reflector, it is possible to achieve aerial imaging with high light utilization efficiency [22]. In this experiment, we used DBEF-Qv2 (manufactured by 3M), whose reflectance changes according to the polarization state of incident light, bonded to a 3 mm thick glass plate as a beam splitter, and RF-Ay (manufactured by Nippon Carbide Industry) as the retro-reflector and add a $\lambda/4$ retardation film on the RF-Ay. As a result, it was confirmed by measurement that the luminance when the white aerial image is 850 cd/m². In addition, in order to conduct experiments under the influence of diffraction, which is the main cause of blurring, the retroreflective material is placed at an angle of 45 degrees when viewed from

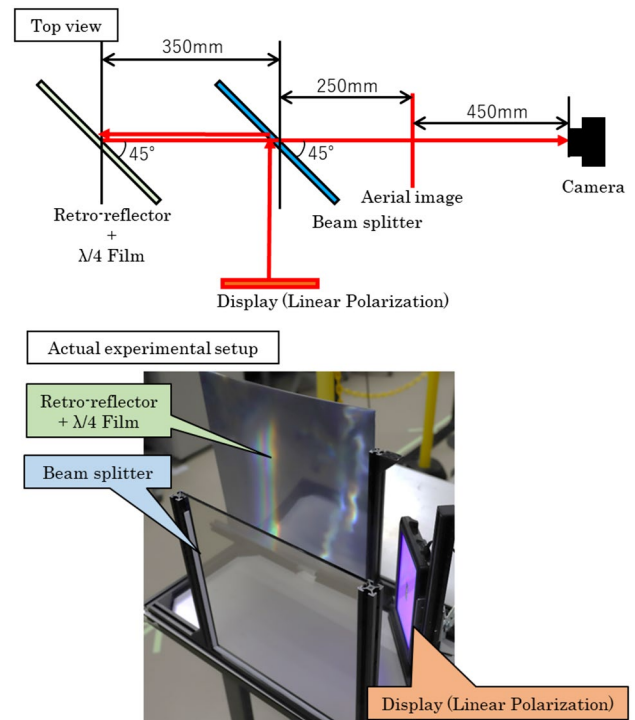


Fig. 5 Experimental setup for PSF measurements

the center of the camera optical axis, and the aperture width of the element is made small. As for the camera device, Canon's EOS6 Mark II was used, and manually focused on the image formation position of the aerial image. The parameters for shooting are set to F: 4.0, shutter speed: 1/10, and ISO 800. The distance from the aerial imaging optical system to the aerial image is set at 250 mm, and the camera is placed at a position further 450 mm away from it. Since the distance between the beam splitter and the retro-reflecting material is 350 mm, the effect of diffraction is such that the imaging light spreads through a distance of 600 mm on the central axis and affects the blurriness.

We measure PSF using three monochromatic test images as comparison parameters in order to measure the change in diffraction that changes according to the magnitude of the wavelength of light. Figure 6 shows the test image used for PSF measurement. We use an image in a circle with a radius of 5 mm, which is a pattern of the three primary colors of red, green, and blue.

3.2 Implementation of aerial image correction system

In this experiment, deconvolution processing is implemented using digital image processing programming in order to give blur correction effects to actual full-color aerial images. Figure 7 shows a processing flow diagram

Fig. 6 Experimental image for color wavelength comparison

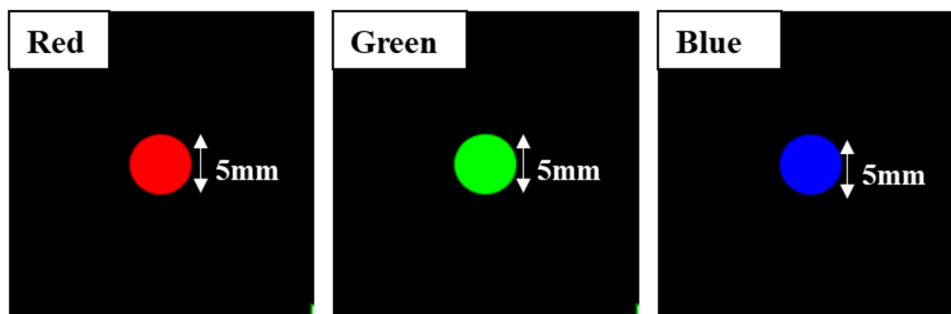
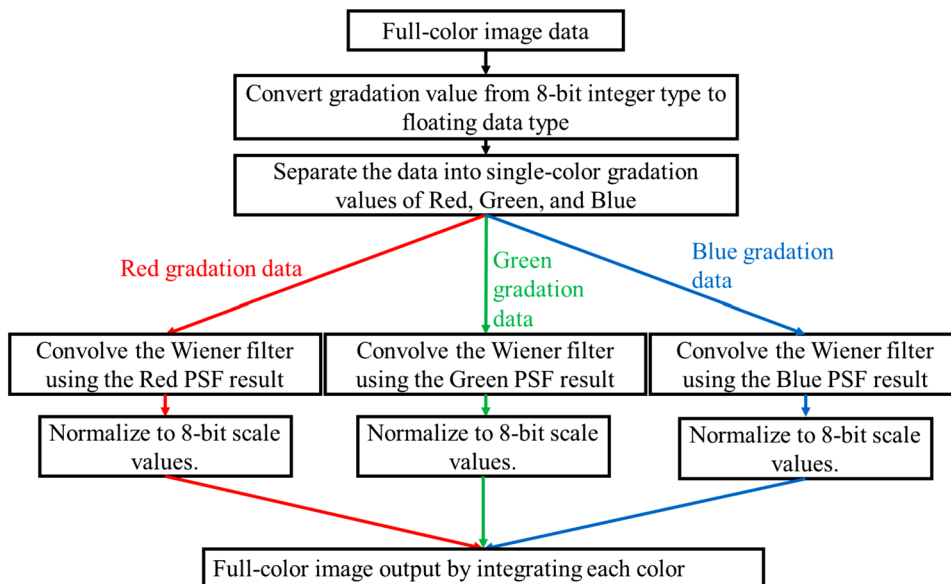


Fig. 7 Correction image processing system flow diagram



for implementing correction processing on the input light source projected onto the aerial image. Blur characteristics vary with color wavelength, as explained in the previous chapter. A digital image converts display colors into data using the three primary colors of red, green, and blue. Therefore, the correction process separates each of the three primary colors from the full-color image data and performs deconvolution on each. Next, digital filtering is realized by digital signal processing using floating-point arithmetic. On the other hand, since the gradation values of normal images are 8-bit integers, they are converted to floating-point numbers before processing and normalized to 8-bit gradation after convolution. In the normalization method of this process, all output values lower than the background are set to 0 and the maximum output values are set to 255 in order to keep the black background portion that should not be affected by the correction effect unchanged. Finally, each color is integrated to output a full-color image. The environment for this implementation is as follows: Windows 10, Core i7 7700K CPU, 16GB memory, C++, and OpenCV3.4.6 library.

4 Results

4.1 Results of PSF due to changes in color wavelength

Figure 8 shows an aerial image set captured for each color wavelength of the light source. It can be qualitatively confirmed that the way the light of the point light source spreads differs depending on the color. The shape of the PSF also changes according to the color tends to expand as the wavelength increases. In addition, it can be seen from the shape of the PSF result that anisotropic blurring occurs due to the special opening shape.

4.2 Results of blur correction of aerial image

In order to check the sharpness of the input image displayed in the aerial image, we prepared two types of single-color characters, each large enough to cause blurring,

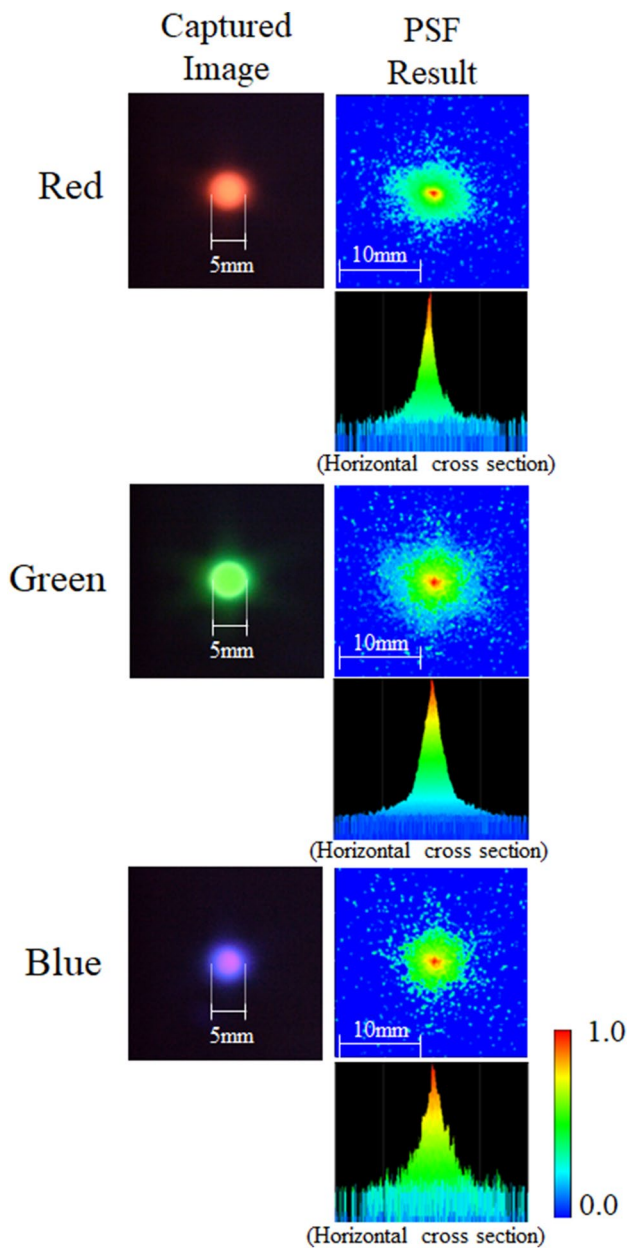


Fig. 8 Captured aerial images and PSF results with varying the color wavelength

as shown in Fig. 9. Also, the correction results for white characters obtained by integrating each single color are similarly compared.

Figure 10 shows the result of capturing an actual aerial image. When the uncorrected image is formed in the air, anisotropic blur similar to that of the PSF in the previous section occurs in the edge region of characters, and it can be confirmed that the sharpness of the characters is reduced. By performing deconvolution processing on the input image before aerial imaging, the single gradation value of the character portion changes, and a directional gradation appears.

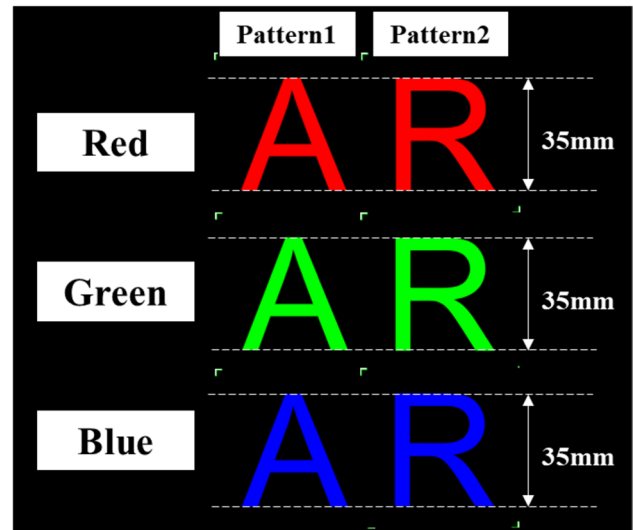


Fig. 9 Light source image for visual evaluation of correction processing

In addition, there is a portion where the luminance gradation is increased outside the boundary between the character and the background. By forming the corrected image as an aerial image, the changed gradation and the blurred light generated by them interfere with each other. As a result, we qualitatively confirmed that the sharpness of the edge regions of characters increased. Also, when white characters are displayed in an aerial image, different blurring occurs for each color wavelength, so it can be confirmed that the color changes near the edge region. Therefore, by integrating the correction results of each color to form a white corrected image, a correction effect is obtained in which the color tone of the edge region becomes uniform during aerial image formation. However, in some areas, it was confirmed that the change in color remained even during aerial imaging.

Next, we compare the effect of correction on actual aerial images with the effect of correction based on the simulation results of previous research [12–14]. The simulation process of the previous research is a deconvolution process performed on the image data of the captured aerial image. An ideal correction effect is assumed because it is performed on imaging data with similar characteristics to the pre-analyzed PSF results. Figure 11 shows the result of comparison with the simulated image. In both resulting images, characteristic correction effects are obtained for each color near the edge regions of characters. On the other hand, the simulated result has a brighter maximum gradation value in the character area and a darker minimum gradation value in the background area than the actual correction result. As for the result of white, the gradation value of each color is higher in the simulation result, and the color is closer to the white of the original image.

Fig. 10 Results of applying deconvolution processing to the aerial images

Specification		Conventional AIRR		Proposed deblur process	
Red	Input image				
	Aerial image				
Green	Input image				
	Aerial image				
Blue	Input image				
	Aerial image				
White	Input image				
	Aerial image				

In order to further analyze the correction results, Fig. 12 shows a histogram of luminance gradation values by setting the region of interest to the edge portion of the character. We set the region of interest to be the area below the horizontal line of the letter “A”, where we can clearly see the change in gradation around the edge region. The size in the region

of interest is 30×80 and the total number of pixels is 2400. In this histogram, there are a low-gradation portion which is a background portion, a high gradation portion which is a character portion, and intermediate gradation corresponding to an edge portion between them. In that uncorrected aerial photograph, the histogram spread is smaller in the order of



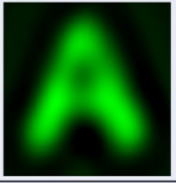

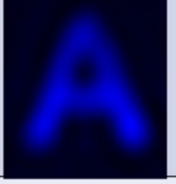
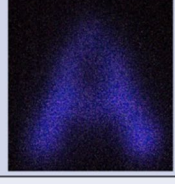


Specification		Simulated Result	Actual aerial image
Red	Aerial image		
Green	Aerial image		
Blue	Aerial image		
White	Aerial image		

Fig. 11 Comparison between simulated results and actual aerial display results in correction processing

blue, red, and green, with widths of 175, 210, and 215. This is because the color gradation value is converted into the luminance value with a coefficient that matches the visual characteristic for each single color. On the other hand, it can be confirmed that the aerial image after correction has fewer intermediate gradations for all colors, and that high gradation portions are distributed at higher luminance values. The width of the histogram is also large for all colors, blue: 185, red: 221, green: 232. This feature indicates that the contrast ratio of the edge region is high. Also, when comparing the simulation results with the results of correcting the actual aerial image, the simulation results show that the distribution of intermediate gradation is extremely small, and the distribution of gradation is lower than that of the low-gradation part. The widths of the histograms are 184 for blue, 228 for red, and 231 for green, which are not significantly different from the actual corrected aerial image. It can be confirmed that, when ideal correction is performed, not only is the contrast ratio in the edge region improved, but also sharpness is achieved without intermediate gradation.

Next, in order to confirm the color change of the white aerial image generated by combining the correction processing of each color, Fig. 13 shows the result of plotting

the white character part with CIE 1931 color spaces. In the diagram of the color space, the line enclosing the boundary of the sRGB color space, which is the standard for digital images, and the white gradation value of maximum luminance are drawn with black circles. The plot results of the aerial image without correction are slightly spread in red and green directions. This is because diffraction is large in the directions of red and green, which have large wavelengths, and the color changes at the edge regions of the characters. The distribution of the plotted results of the actual aerial image with correction spreads further in the direction of red than without correction. It can be confirmed that even when average, median, and variance values of all pixels are compared, the distribution is wider with correction, and there is more distribution in the positive direction of x . In addition, the simulation results show that the dispersion is less than before the correction, and the white color is closer to the ideal white color. It can be seen that although the correction parameters can ideally correct white, ideal correction cannot be achieved in the correction of the actual aerial image.

5 Discussion

We examine the validity of the blur correction process using the deconvolution function, and clarify the system requirements for applying it as a digital image processing system to the aerial display device. Experimental results show that the implemented correction process reduces halftones in the edge region and realizes aerial image with high contrast ratio. However, compared to the original image, the blurring of the edge region cannot be completely removed, and the correction effect differs for each color. We attribute this problem to ideal correction errors in image processing. One of the errors exists in the PSF calculation. In this system, in order to measure the PSF of the light source environment actually displayed in the air, the PSF is created by displaying it on a light source display that uses a circular image with a radius of 5 mm. When the distance between the pixels of a circular image is the longest, and when measuring the difference in three-dimensional angle of incidence when light rays directed from the same camera shooting position to two aerial imaging points are incident on a retro-reflector, there is a relative difference of about 14 degrees between the input angles to the retro-reflector at the two points. In the PSF results shown in the previous study [12], there was a difference in the profile even when the angle of the retroreflector was changed by 15 degrees. In particular, in the case of an error that spreads the PSF with a higher anisotropy, there is a possibility that a spread larger than the size of the filter used in this experiment will occur, and there is a possibility that it cannot be corrected. Therefore, the characteristic that the imaging position differs in mm units appears as an

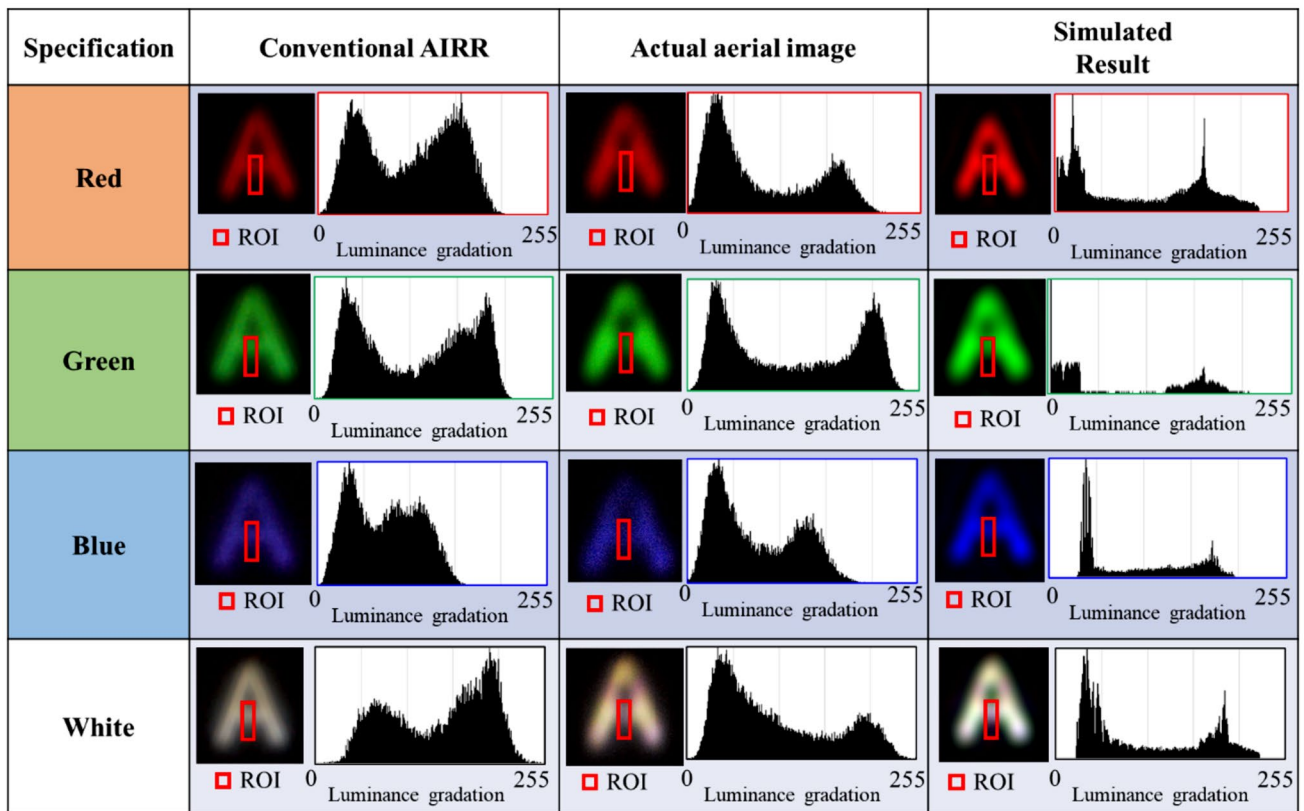


Fig. 12 Luminance histogram result in edge area of aerial image

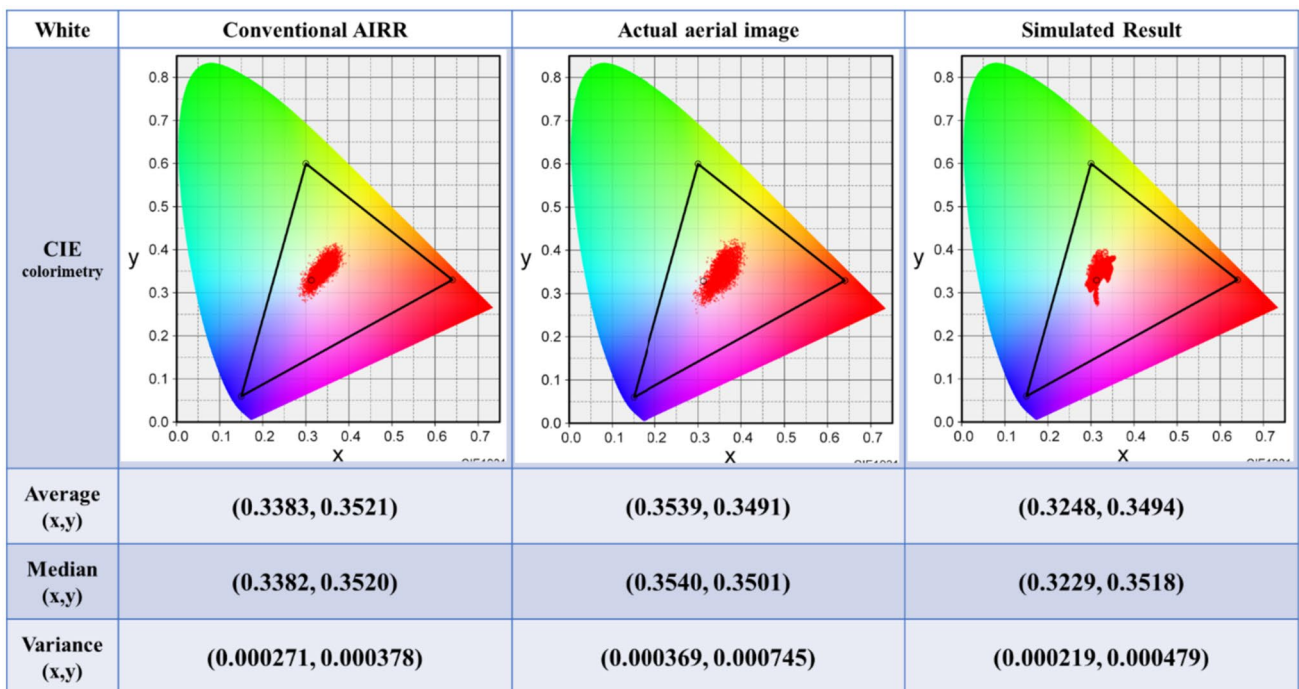


Fig. 13 Chromaticity changes due to white blur correction effect

error in the PSF. In addition, since the character image to be corrected also includes an imaging optical path different from the position measured by the PSF, the correction effect varies.

Another factor is the error in the deconvolution process. The size of the correction filter obtained from the PSF results depends on the pixel pitch of the display. In this experiment, the filter size is 650×650 , which can correct the effects of blurring up to about 5mm. Therefore, large blurs larger than the filter size and finer blurs smaller than the pixel pitch cannot be corrected. Furthermore, precision errors smaller than the pixel pitch may affect the uniformity of displayed colors and edge distortion, and appear as qualitative visual discomfort rather than quantitative performance. In addition, since the gradation value of a general display device is 8 bits, quantization error is also a cause of error. The quantization error includes the error caused by normalizing a numerical value that is output as a negative value by filtering to 0. Ideal correction processing requires not only correction on the character area side, but also correction obtained by making the background area darker. In order to perform this correction on an actual aerial image, it is necessary to normalize the image space including the background area involved in the correction process using the minimum and maximum values of the filtering process output results.

Furthermore, from the results of comparison with the simulation results, the simulation results show that the highest brightness part is higher, the lowest brightness component is at a lower position, and the peaks of the histogram are more concentrated. This suggests that the correction for the actual aerial image is insufficient for the intermediate gradation component. From the result of the white color change shown in Fig. 13, it can be confirmed that the red component is more visible than the ideal correction result. Therefore, in the correction process, the brightness level is corrected in accordance with the wavelength so that correction closer to the original image can be achieved. In this experimental environment, an ideal white color can be displayed by performing a correction that attenuates the red gradation component. Also, in terms of image processing, a factor that causes this problem is the correction limit for low-gradation values. The original deconvolution process also suppresses pixel gradation that increases brightness due to blur not only in high-brightness areas but also in low-brightness areas of the background. In the simulation result, the brightness of the background portion has already increased due to the blurring, so it is appropriately corrected. However, when the input image is corrected in advance, the background portion is 0, which is the lowest digital value, and therefore is not corrected appropriately. In order to solve this, it is necessary to set the brightness of the background part to a value greater than 0 in advance. In addition, as future research aimed at improving correction processing,

it is necessary to construct a simulator environment that can reproduce the image quality and correction effects of actual aerial images, and to optimize processing parameters in virtual space. To achieve this, our future work will be to construct a simulation environment that reproduces the actual correction processing procedures and parameters, including the aerial imaging optical system.

Based on these considerations, there are several ways to increase the effectiveness of the image correction method in this paper for improving visibility. For example, implementing additional corrections to the deconvolution process. Based on the obtained PSF results, the locations where blurring changes are estimated for the input content, an additional correction processing is performed on those locations to achieve uniform resolution throughout the content. These processes can be realized by adjusting using the noise function set when generating the Wiener filter, or by implementing another filter function. Also, as a solution to the correction limit of the low-luminance portion described above, it is considered effective to incorporate control for raising the low-gradation pixels to which the filter is applied.

Furthermore, the aerial display product requires a dynamic image processing system. In this experiment, the positional relationship between the camera and the constituent optical members was fixed. However, in an actual floating display device, the imaging optical path changes according to the user's viewpoint position, and the blur characteristics also change. Therefore, it is necessary to dynamically change the correction filter in cooperation with a detection system that identifies the user's viewpoint position, such as a camera sensor.

6 Conclusion

We implemented an image processing system that analyzes the blur according to the color wavelength peculiar to AIRR and corrects the blur with the actual aerial image. In addition, the correction effect was verified by taking an actual aerial image and comparing it with the simulation result. As a result, it was confirmed that the contrast ratio in the edge region improved compared to before correction, and the visibility improved by the correction processing that matched the blurring that changed for each color.

On the other hand, compared with the ideal simulation results, it was found that errors in the image processing system affected the correction effect. In future, in order to apply this technology to the display system of the aerial display device, it is necessary to implement a system that responds to changes in the video content and the user's viewpoint position, such as interlocking with the detection system and dynamic filter correction processing. We will proceed with research with the aim of applying this technology as a new

display solution that connects the digital space and the real space in future.

Author contributions HK contributed for this paper as 1st author. He designed and conducted the experiments, analyzed the data and wrote the original draft. MY and HY designed and analyzed the experiments, and edited the manuscript.

Funding Funding was provided by Japan Society for the Promotion of Science (grant no. 20H05702).

Data availability Data underlying the results presented in this paper are not publicly available at this time but may be obtained from the authors upon reasonable request.

Declarations

Conflict of interest The authors declare no conflicts of interest associated with this manuscript.

References

- Hong, J., Kim, Y., Choi, H.-J., Hahn, J., Park, J.-H., Kim, H., Min, S.-W., Chen, N., Lee, B.: Three-dimensional display technologies of recent interest: principles, status, and issues. *Appl. Opt.* **50**(34), H87–H115 (2011)
- Geng, J.: Three-dimensional display technologies. *Adv. Opt. Photon.* **5**(4), 456–535 (2013)
- Yole Developpement: Report, next generation 3d display. http://www.yole.fr/iso_upload/News/2019/PR_NEXT_GENERATION_3D_DISPLAY_OverviewYOLE_October2019.pdf. Accessed 2 Sept 2021
- Mitsubishi Electric Corp: News release. <http://www.mitsubishi-electric.com/news/2016/0217-e.html>. Accessed 2 Sept 2021
- Tokuda, Y., Hiyama, A., Hirose, M., Yamamoto, H.: R2D2 w/ AIRR: real time & real space double-layered display with aerial imaging by retro-reflection. In: *Proc. SIGGRAPH Asia'15, Emerging Technologies*, pp. 20:1–20:3 (2015)
- Matsuura, Y., Koizumi, N.: A method of scooping mid-air images on water surface. In: *Proceedings of the 2018 ACM International Conference on Interactive Surfaces and Spaces*, pp. 227–235 (2018)
- Miyazaki, D., Maeda, Y., Maekawa, S.: Floating three-dimensional image display using micro-mirror array imaging element. *Proc. SPIE* **9495**, 949508–949512 (2018)
- Maekawa, S., Markon, S.: Airflow interaction with Floating images. In: *SIGGRAPH ASIA 2009 Art Gallery & Emerging Technologies. SIGGRAPH ASIA'09 Art Gallery & Emerging Technologies*, p. 61 (2009)
- Ueda, Y., Iwazaki, K., Shibasaki, M., Mizushina, Y., Furukawa, M., Nii, H., Minamizawa, K., Tachi, S.: Mid-air autostereoscopic display for seamless interaction with mixed reality environments. In: *Proceedings of SIGGRAPH'14, Emerging Technologies*, p. 10:1 (2014).
- Suginohara, H., Kikuta, H., Nakamura, Y., Minami, K., Yamamoto, H.: An aerial display: passing through a floating image formed by retro-reflective reimaging. *SID Symp. Digest Tech. Pap.* **48**, 406–409 (2017)
- Miyazaki, D., Onoda, S., Maeda, Y., Mukai, T.: Blurring correction for aerial image formed by dihedral corner reflector array. In: *CLEO Pacific Rim*, paper 25B1_3 (2015)
- Kikuta, H., Yasugi, M., Yamamoto, H.: Examination of deblur processing according to optical parameters in aerial image. *OSA Contin.* **1**(3), 462–474 (2022)
- Kikuta, H., Yasugi, M., Yamamoto, H.: Quantitative comparisons of deconvolution processing to deblur aerial image formed with aerial imaging by retro-reflection. In: *The 11th Laser Display and Lighting Conference 2022*, pp. LDC-8-04 (2022)
- Kikuta, H., Yasugi, M., Yamamoto, H.: Optimization of blur correction of color images formed with aerial imaging by retro-reflection. *Opt. Rev.* **30**(1), 111–121 (2023)
- Kikuta, H., Yasugi, M., Yamamoto, H.: Image processing system for blur correction of aerial imaging by retro-reflection. In: *The 12th Laser Display and Lighting Conference 2023*, p. LDC-7-04 (2023)
- Burckhardt, C.B., Collier, R.J., Doherty, E.T.: Formation and inversion of pseudoscopic images. *Appl. Opt.* **7**, 627–631 (1968)
- Yamamoto, H., Suyama, S.: Aerial imaging by retro-reflection (AIRR). In: *SID'13 DIGEST*, 895 (2013)
- Yamamoto, H., Tomiyama, Y., Suyama, S.: Floating aerial LED signage based on aerial imaging by retro-reflection (AIRR). *Opt. Express* **22**, 26919–26924 (2014)
- Maekawa, S., Nitta, K., Matoba, O.: Advances in passive imaging elements with micromirror array. *Proc. SPIE* **6392**, 63920E (2006)
- ASKA 3D: <https://aska3d.com/en/technology.html>. Accessed 2 Sept 2021
- Zhang, R., Hua, H.: Imaging quality of a retroreflective screen in head-mounted projection display. *J. Opt. Soc. Am. A* **26**(5), 1240–1249 (2009)
- Fujii, K., Endo, N., Hagen, N., Yasugi, M., Suyama, S., Yamamoto, H.: Aerial video-calling system with eye-matching feature based on polarization-modulated aerial imaging by retro-reflection (p-AIRR). *Opt. Rev.* **29**(1), 429–439 (2022)

Publisher's Note Springer Nature remains neutral with regard to jurisdictional claims in published maps and institutional affiliations.

Springer Nature or its licensor (e.g. a society or other partner) holds exclusive rights to this article under a publishing agreement with the author(s) or other rightsholder(s); author self-archiving of the accepted manuscript version of this article is solely governed by the terms of such publishing agreement and applicable law.